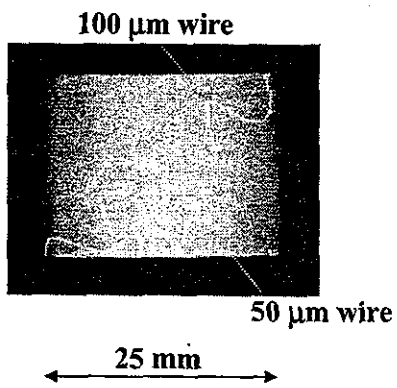

FIG. 7. Radiograms of tungsten wires in a PMMA rod with a tube voltage of 60 kV.

spheres of 15 μm in diameter at a tube voltage of 60 kV. The iodine spheres contained 37% iodine by weight, and the cerium spheres contained 18% cerium by weight. The concentration of spheres in the blood varies with the filling rate, and the estimated densities of the iodine and the cerium of blood are less than 0.44 and 0.17 g/cm^3, respectively. In the case where the cerium spheres were employed, the coronary arteries were barely visible. Figure 9(a) shows an angiogram of a larger dog heart using the cerium target at a tube voltage of 60 kV using iodine spheres. For comparison, we performed angiography with a tungsten x-ray tube at a tube voltage of 60 kV [Fig. 9(b)].

If we assume that the filling rate of the iodine microspheres in a blood vessel is constant, the image contrast of the blood is in inverse proportion to the vessel diameter. Next, the density ratios (maximum density divided by minimum density) obtained by the cerium and tungsten tubes were 4.3 and 2.7, respectively. In angiography using the tungsten target, blood vessels of approximately 100 μm were hardly observed at all.

V. DISCUSSION

In summary, we developed a x-ray generator with a cerium-target tube and succeeded in producing cerium $K\alpha$ lines, which can be absorbed easily by iodine-based contrast mediums. Both the characteristic and bremsstrahlung x-ray

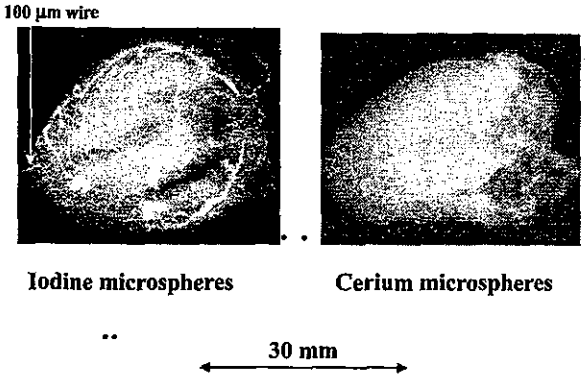

FIG. 8. Angiograms of extracted rabbit hearts using iodine and cerium microspheres with a tube voltage of 60 kV.

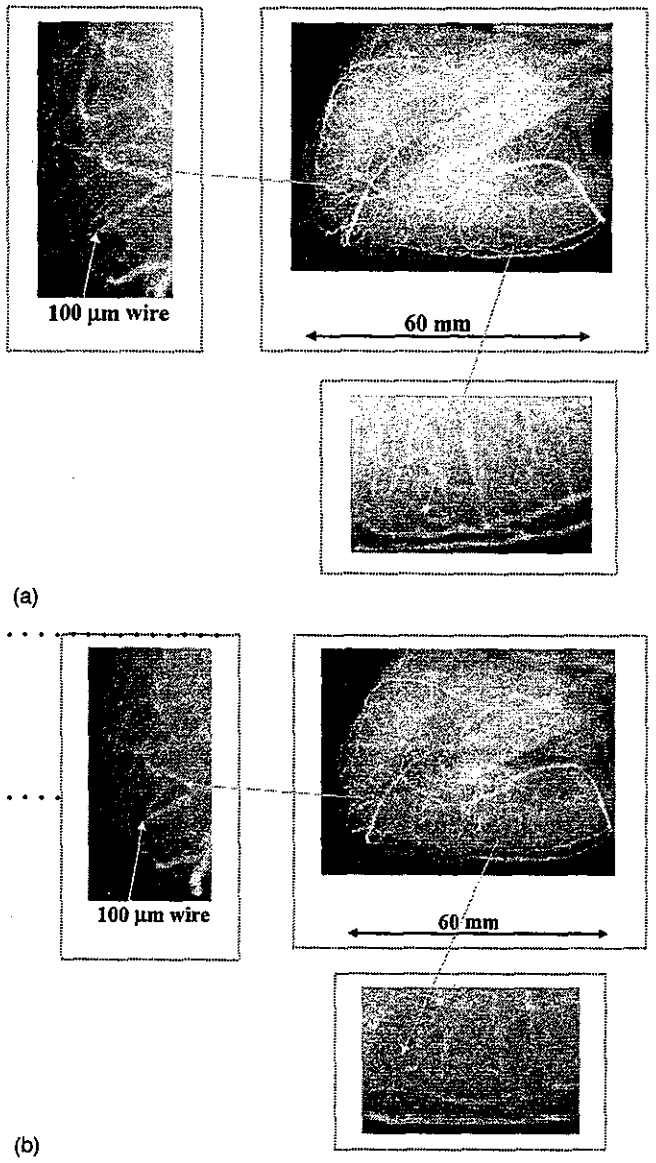

FIG. 9. Angiograms of an extracted dog heart achieved with (a) cerium and (b) tungsten target x-ray tubes using iodine microspheres with a tube voltage of 60 kV.

intensities increased with increases in the tube voltage, and $K\beta$ lines were absorbed effectively by the barium sulfate filter. The x-ray intensity was limited because the thermal contact between the target and the anode was not good. However, the intensity can be increased by welding the target or using a cerium-alloy target.

In this preliminary experiment, although the maximum tube voltage and current were 65 kV and 0.40 mA, respectively, the voltage and current could be increased. Subsequently, the generator produced maximum number of characteristic photons was approximately 3×10^7 photons/cm^2 s at 1.0 m from the source, and the photon count rate can be increased easily by improving the target.

Since the sampling pitch of the CR system is 87.5 μm, we obtained resolutions of approximately 100 μm, and high-contrast blood vessels could be observed using a CR system. In order to observe fine blood vessels of less than 100 μm,

the image resolution of the CR system should be improved as much as possible, and a flat panel system is useful to observe blood flows for cases of cardiovascular disease.

ACKNOWLEDGMENTS

This work was supported by Grants-in-Aid for Scientific Research and Advanced Medical Scientific Research from MECSST (13470154, 13877114, and 16591222), Grants from Keiryo Research Foundation, JST (Test of Fostering Potential), NEDO, and MHLW (HLSRG, RAMT-nano-001, RHGTEFB-genome-005, and RGCD13C-1).

[a]Author to whom correspondence should be addressed. Department of Physics, Iwate Medical University, 3-16-1 Honchodori, Morioka 020-0015, Japan; electronic mail: dresato@iwate-med.ac.jp

[1]A. Akisada, M. Ando, K. Hyodo, S. Hasegawa, K. Konishi, K. Nishimura, A. Maruhashi, F. Toyofuku, A. Suwa, and K. Kohra, "An attempt at coronary angiography with a large size monochromatic SR beam," Nucl. Instrum. Methods Phys. Res. A **246**, 713–718 (1986).

[2]A. C. Thompson, H. D. Zeman, G. S. Brown, J. Morrison, P. Reiser, V. Padmanabahn, L. Ong, S. Green, J. Giacomini, H. Gordon, and E. Rubenstein, "First operation of the medical research facility at the NSLS for coronary angiography," Rev. Sci. Instrum. **63**, 625–628 (1992).

[3]H. Mori, K. Hyodo, E. Tanaka, M. U. Mohammed, A. Yamakawa, Y. Shinozaki, H. Nakazawa, Y. Tanaka, T. Sekka, Y. Iwata, S. Honda, K. Umetani, H. Ueki, T. Yokoyama, K. Tanioka, M. Kubota, H. Hosaka, N. Ishizawa, and M. Ando, "Small-vessel radiography in situ with monochromatic synchrotoron radiation," Radiology **201**, 173–177 (1996).

[4]K. Hyodo, M. Ando, Y. Oku, S. Yamamoto, T. Takeda, Y. Itai, S. Ohtsuka, Y. Sugishita, and J. Tada, "Development of a two-dimensional imaging system for clinical applications of intravenous coronary angiography using intense synchrotron radiation produced by a multipole wiggler," J. Synchrotron Radiat. **5**, 1123–1126 (1998).

[5]R. Germer, "X-ray flash techniques," J. Phys. E **12**, 336–350 (1979).

[6]E. Sato, H. Isobe, and F. Hoshino, "High intensity flash x-ray apparatus for biomedical radiography," Rev. Sci. Instrum. **57**, 1399–1408 (1986).

[7]E. Sato, S. Kimura, S. Kawasaki, H. Isobe, K. Takahashi, Y. Tamakawa, and T. Yanagisawa, "Repetitive flash x-ray generator utilizing a simple diode with a new type of energy-selective function," Rev. Sci. Instrum. **61**, 2343–2348 (1990).

[8]A. Shikoda, E. Sato, M. Sagae, T. Oizumi, Y. Tamakawa, and T. Yanagisawa, "Repetitive flash x-ray generator having a high-durability diode driven by a two-cable-type line pulser," Rev. Sci. Instrum. **65**, 850–856 (1994).

[9]E. Sato, K. Takahashi, M. Sagae, S. Kimura, T. Oizumi, Y. Hayasi, Y. Tamakawa, and T. Yanagisawa, "Sub-kilohertz flash x-ray generator utilizing a glass-enclosed cold-cathode triode," Med. Biol. Eng. Comput. **32**, 289–294 (1994).

[10]K. Takahashi, E. Sato, M. Sagae, T. Oizumi, Y. Tamakawa, and T. Yanagisawa, "Fundamental study on a long-duration flash x-ray generator with a surface-discharge triode," Jpn. J. Appl. Phys., Part 1 **33**, 4146–4151 (1994).

[11]E. Sato, M. Sagae, K. Takahashi, A. Shikoda, T. Oizumi, Y. Hayasi, Y. Tamakawa, and T. Yanagisawa, "10 kHz microsecond pulsed x-ray generator utilizing a hot-cathode triode with variable durations for biomedical radiography," Med. Biol. Eng. Comput. **32**, 295–301 (1994).

[12]E. Sato, Y. Hayasi, R. Germer, E. Tanaka, H. Mori, T. Kawai, T. Ichimaru, K. Takayama, and H. Ido, "Quasi-monochromatic flash x-ray generator utilizing weakly ionized linear copper plasma," Rev. Sci. Instrum. **74**, 5236–5240 (2003).

[13]E. Sato, Y. Hayasi, R. Germer, E. Tanaka, H. Mori, T. Kawai, H. Obara, T. Ichimaru, K. Takayama, and H. Ido, "Irradiation of intense characteristic x-rays from weakly ionized linear molybdenum plasma," Jpn. J. Med. Phys. **23**, 123–131 (2003).

[14]M. Sonoda, M. Takano, J. Miyahara, and H. Kato, "Computed radiography utilizing scanning laser stimulated luminescence," Radiology **148**, 833–838 (1983).

[15]E. Sato, K. Sato, and Y. Tamakawa, "Film-less computed radiography system for high-speed imaging," Ann. Rep. Iwate Med. Univ. Sch. Lib. Arts and Sci. **35**, 13–23 (2000).

Weakly ionized cerium plasma radiography

Eiichi Sato[a], Yasuomi Hayasi[a], Rudolf Germer[b], Yoshitake Koorikawa[a], Kazunori Murakami[a], Etsuro Tanaka[c], Hidezo Mori[d], Toshiaki Kawai[e], Toshio Ichimaru[f], Fumiko Obata[g], Kiyomi Takahashi[g], Sigehiro Sato[g], Kazuyoshi Takayama[h] and Hideaki Ido[i]

[a]Department of Physics, Iwate Medical University, 3-16-1 Honchodori, Morioka 020-0015, Japan
[b]ITP, FHTW FB1 and TU-Berlin, Blankenhainer Str. 9, D 12249 Berlin, Germany
[c]Department of Nutritional Science, Faculty of Applied Bio-science, Tokyo University of Agriculture, 1-1-1 Sakuragaoka, Setagaya-ku 156-8502, Japan
[d] Department of Cardiac Physiology, National Cardiovascular Center Research Institute, 5-7-1 Fujishiro-dai, Suita, Osaka 565-8565, Japan
[e]Electron Tube Division #2, Hamamatsu Photonics Inc., 314-5 Shimokanzo, Toyooka Village, Iwata-gun 438-0193, Japan
[f] Department of Radiological Technology, School of Health Sciences, Hirosaki University, 66-1 Honcho, Hirosaki 036-8564, Japan
[g]Department of Microbiology, School of Medicine, Iwate Medical University, 19-1 Uchimaru, Morioka 020-8505, Japan
[h]Shock Wave Research Center, Institute of Fluid Science, Tohoku University, 2-1-1 Katahira, Aoba-ku, Sendai 980-8577, Japan
[i] Department of Applied Physics, Faculty of Engineering, Tohoku Gakuin University, 1-13-1 Chuo, Tagajo 985-8537, Japan

ABSTRACT

In the plasma flash x-ray generator, high-voltage main condenser of about 200 nF is charged up to 55 kV by a power supply, and electric charges in the condenser are discharged to an x-ray tube after triggering the cathode electrode. The flash x-rays are then produced. The x-ray tube is of a demountable triode that is connected to a turbo molecular pump with a pressure of approximately 1 mPa. As electron flows from the cathode electrode are roughly converged to a rod cerium target of 3.0 mm in diameter by electric field in the x-ray tube, the weakly ionized linear plasma, which consists of cerium ions and electrons, forms by target evaporating. At a charging voltage of 55 kV, the maximum tube voltage was almost equal to the charging voltage of the main condenser, and the peak current was about 20 kA. When the charging voltage was increased, weakly ionized cerium plasma formed, and the K-series characteristic x-ray intensities increased. The x-ray pulse widths were about 500 ns, and the time-integrated x-ray intensity had a value of about 40 μC/kg at 1.0 m from x-ray source with a charging voltage of 55 kV. In the angiography, we employed a film-less computed radiography (CR) system and iodine-based microspheres. Because K-series characteristic x-rays are absorbed easily by the microspheres, high-contrast angiography has been performed.

Key words: Plasma x-ray, cerium target, weakly ionized cerium plasma, characteristic x-ray, high contrast angiography

Ultrahigh- and High-Speed Photography, Photonics, and Videography, edited by Donald R. Snyder, Proc. of SPIE Vol. 5210 (SPIE, Bellingham, WA, 2004) · 0277-786X/04/$15 · doi: 10.1117/12.506563

1. INTRODUCTION

Flash x-rays are useful in order to perform high-speed radiography, and various generators have been developed to correspond to specific radiographic objectives.[1-6] In the cases of multiple-shot and cine radiographies, we have developed several different repetitive-flash[7-11] and stroboscopic x-ray generators.[12-18] Although most flash x-ray generators have cold-cathode tubes, the stroboscopic generators utilize hot-cathode tubes.

In conjunction with single crystals, synchrotrons generate monochromatic x-rays. These rays play important roles in parallel radiography and have been employed to perform high-contrast micro-angiography[19] and x-ray phase imaging.[20,21] However, it is difficult to obtain sufficient machine times for various research projects including medical applications.

As for angiography using iodine-based contrast mediums, K-series characteristic x-rays of cerium are extremely useful, since the rays are absorbed easily by iodine. In particular, since quite intense and sharp characteristic x-rays have been produced from weakly ionized linear plasmas[22-25] of nickel, copper and molybdenum, the development of a cerium-target x-ray tube for angiography is highly desirable.

In this research, we developed a single flash x-ray generator with a cerium-target plasma tube and performed a tentative study on weakly ionized cerium plasma angiography.

2. GENERATOR

2.1 High-voltage circuit

Figure 1 shows block diagram of a high-intensity plasma flash x-ray generator. This generator consists of the following essential components: a high-voltage power supply, a high-voltage condenser with a capacity of about 200 nF, a turbo-molecular pump, a krytron pulse generator as a trigger device, and a flash x-ray tube. In this generator, a low-impedance transmission line is employed in order to increase maximum tube current. The high-voltage main condenser is charged up to 55 kV by the power supply, and electric charges in the condenser are discharged to the tube after triggering the cathode electrode by the trigger device. The plasma flash x-rays are then produced.

2.2 X-ray tube

The x-ray tube is a demountable cold-cathode triode that is connected to the turbo molecular pump with a pressure of approximately 1 mPa (Fig. 2). This tube consists of the following major parts: a pipe-shaped carbon cathode with a bore diameter of 10.0 mm, a trigger electrode made from a copper wire, a stainless-steel vacuum chamber, a nylon insulator, a polyethylene terephthalate (Mylar) x-ray window of 0.25 mm, and a rod-shaped cerium target of 3.0 mm in diameter. The target tip is embedded in the carbon rod in order to absorb the characteristic x-rays of carbon by the window. The distance between the target and cathode electrodes is approximately 20 mm, and the trigger electrode is set in the cathode electrode. As electron beams from the cathode electrode are roughly converged to the target by electric field in the tube, the weakly ionized plasma, which consists of cerium ions and electrons, forms around the target by evaporating.

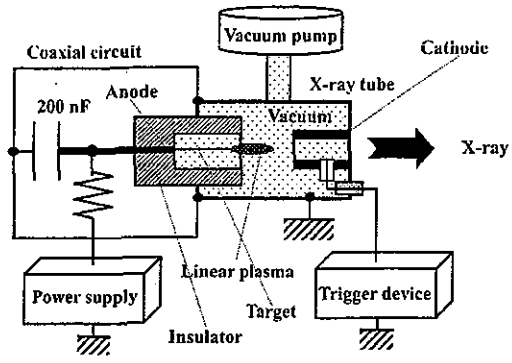

Figure 1: Block diagram of high-intensity plasma flash x-ray generator.

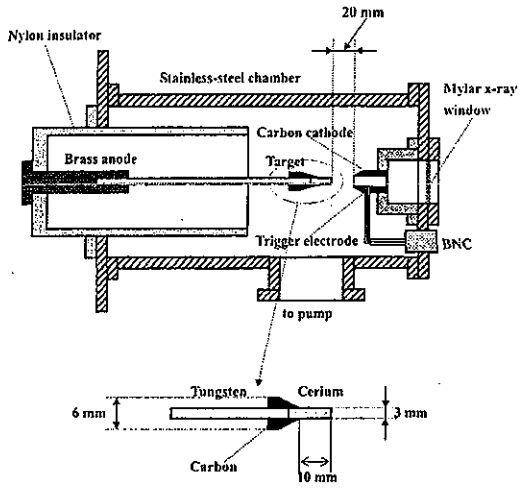

Figure 2: Schematic drawing of flash x-ray tube with a rod target.

3. CHARACTERISTICS

3.1 Tube voltage and current

Tube voltage and current were measured by a high-voltage divider with an input impedance of 1 GΩ and a current transformer, respectively. Figure 3 shows time relation between the tube voltage and current. At the indicated charging voltages, they roughly displayed damped oscillations. When the charging voltage was increased, both the maximum tube voltage and current increased. At a charging voltage of 55 kV, the maximum tube voltage was almost equal to the charging voltage of the main condenser, and the maximum tube current was about 20 kA.

3.2 X-ray output

X-ray output pulse was detected using a combination of a plastic scintillator and a photomultiplier. The x-ray pulse height substantially increased with corresponding increases in the charging voltage (Fig. 4). The x-ray pulse widths were about 500 ns, and the time-integrated x-ray intensity measured by a thermoluminescence dosimeter (Kyokko TLD Reader 1500 utilizing MSO-S elements without energy compensation) had a value of about 40 μC/kg at 1.0 m from the x-ray source with a charging voltage of 55 kV.

3.3 X-ray source

In order to measure images of the plasma x-ray source, we employed a pinhole camera with a hole diameter of 100 μm (Fig. 5). When the charging voltage was increased, the plasma x-ray source grew, and both spot dimension and intensity increased. In contrast, both the dimension and intensity decreased according to insertion of the monochromatic filter.

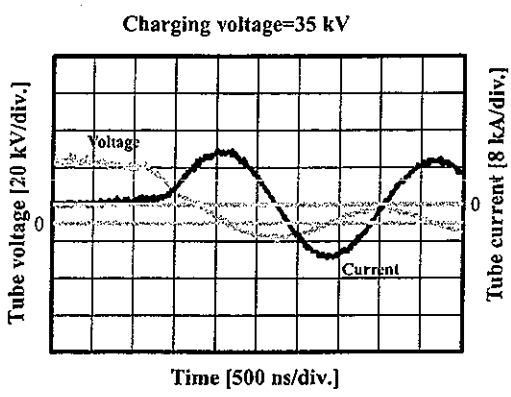

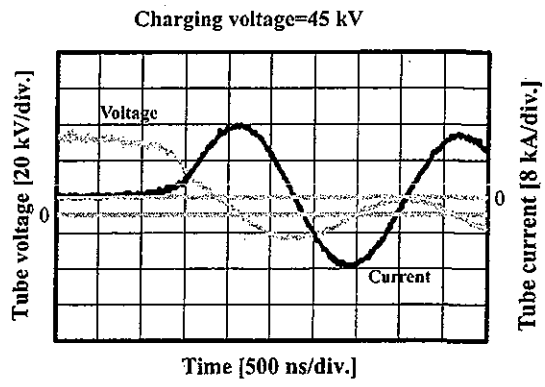

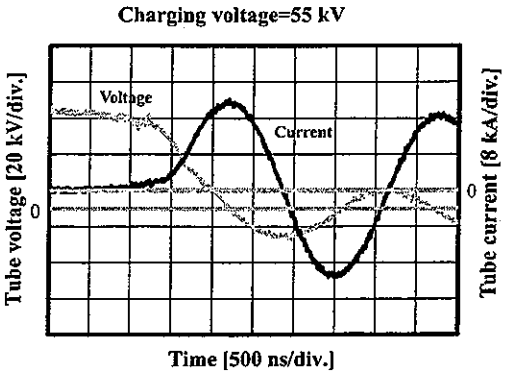

Figure 3: Tube voltages and currents at the indicated charging voltages.

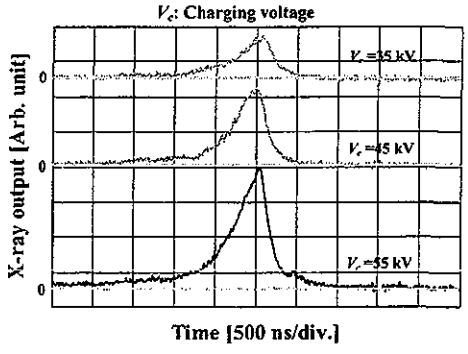

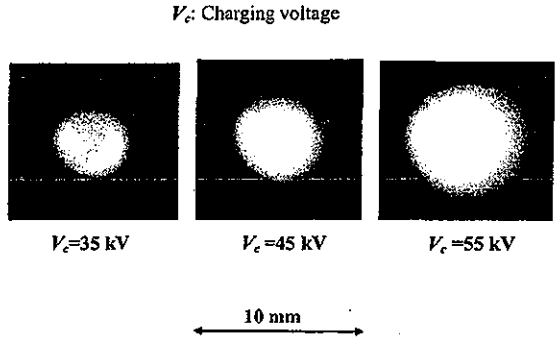

Figure 4: X-ray outputs at the indicated conditions.

Figure 5: Images of plasma x-ray source.

3.4 X-ray spectra

X-ray spectra from the plasma source were measured by a transmission-type spectrometer with a lithium fluoride curved crystal of 0.5 mm in thickness (Fig. 6). The spectra were taken by a computed radiography (CR) system[26] (Konica Regius 150) having a wide dynamic range, and relative x-ray intensity was calculated from Dicom digital data. Figure 7 shows measured spectra from the cerium target. In this experiment, although we observed both the bremsstrahlung and characteristic x-rays, we could not observe characteristic x-rays with a charging voltage of 35 kV

because the critical excitation energy is 40.3 keV. Both the intensities increased substantially with increases in the charging voltage.

3.5 X-ray divergence by slits

In order to ascertain difference of characteristics between x-rays from a conventional tube and these from the plasma tube, we employed two lead slits in order to measure the divergence of the x-rays (Fig. 8). As compared with x-rays from a conventional tube having a tungsten target, the characteristic x-rays from the plasma were diffused greatly after passing through two slits (Fig. 9).

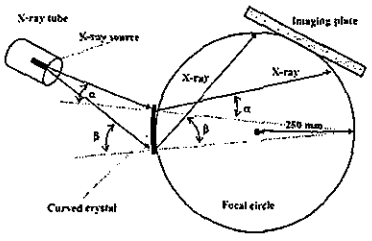

Figure 6: Transmission-type spectrometer with a lithium fluoride curved crystal and an imaging plate.

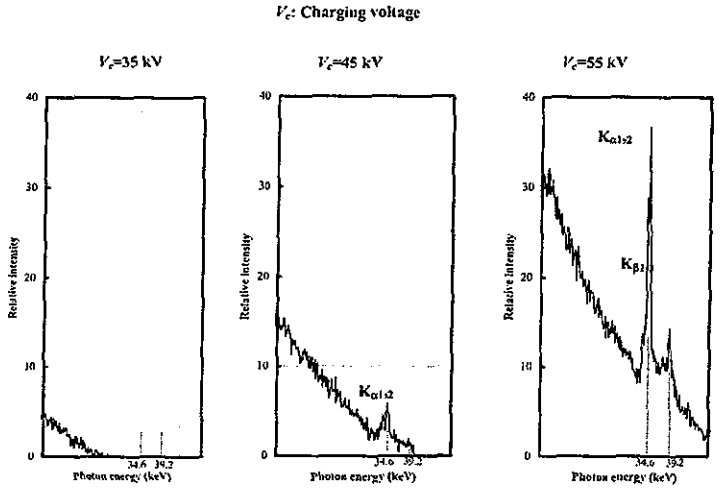

Figure 7: X-ray spectra from weakly ionized cerium plasma.

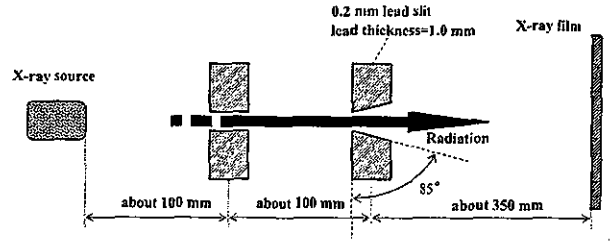

Figure 8: Experimental setup for measuring x-ray divergence using two lead slits.

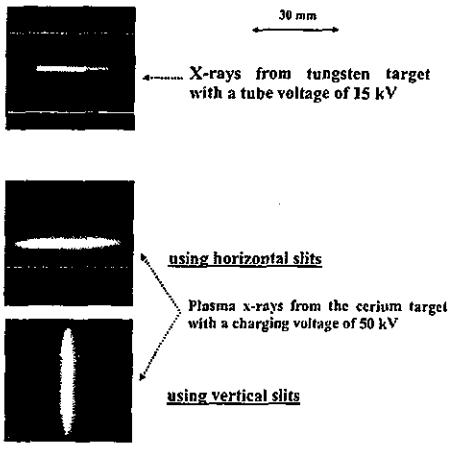

Figure 9: X-ray divergence by two lead slits.

4. ANGIOGRAPHY

The plasma angiography was performed by the CR system without using a monochromatic filter, and the distance between the x-ray source and the imaging plate was 1.2 m.

Firstly, rough measurements of image resolution were made using wires. Figure 10 shows radiograms of 50 μm-diameter tungsten wires coiled around a pipe and a rod made of polymethyl methacrylate (PMMA) with a charging voltage of 55 kV. Although the image contrast increased using the pipe, *50 μm-diameter wires could be* observed.

The image of water falling into a polypropylene beaker from a glass test tube is shown in Fig. 11. This image was taken with a charging voltage of *55 kV, with the slight addition of an iodine-based* contrast medium. Because the x-ray duration was about 1 μs, the stop-motion image of water could be obtained.

Angiograms of rabbit hearts are shown in Fig. 12. These two images were obtained using iodine and cerium *microspheres of 20 μm, respectively,* with a charging voltage of 55 kV. In case where the cerium spheres were employed, the coronary arteries were barely visible. Figure 13 shows an angiogram of the external ear of a rabbit using iodine spheres with a charging voltage of 55 kV, and fine blood vessels of about *50 μm are clearly visible. In* angiography of a larger heart extracted from a dog, using iodine spheres, a PMMA plate was set in front of heart facing x-ray source, and image contrast of coronary arteries increased with increases in the plate thickness (Fig. 14).

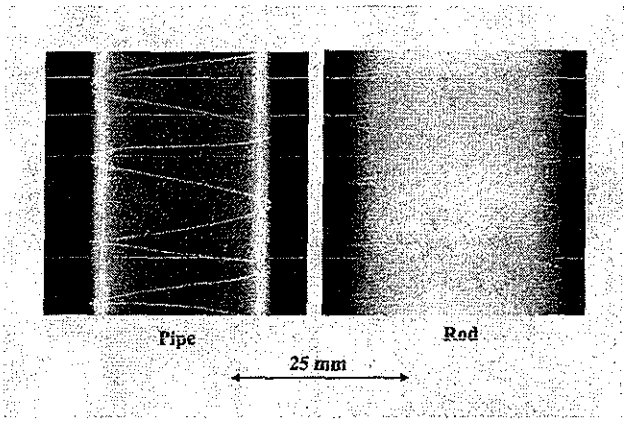

Figure 10: Radiograms of tungsten wires of 50 μm in diameter coiled around pie and a rod made of PMMA.

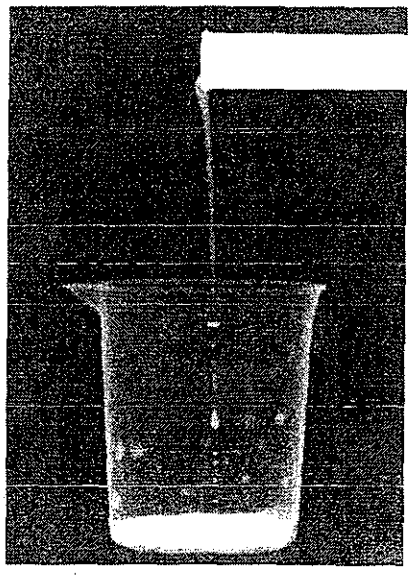

Figure 11: Radiogram of water falling into a polypropylene beaker from a glass test tube.

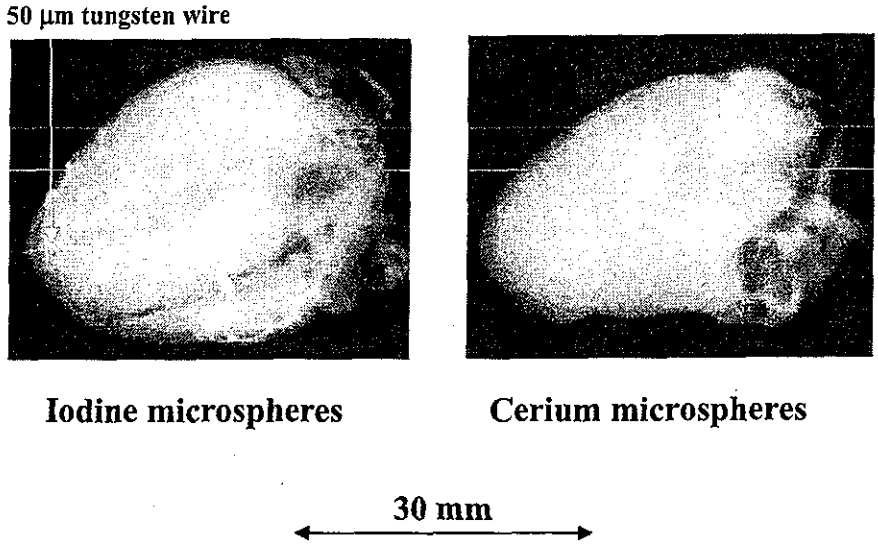

Figure 12: Angiograms of rabbit hearts using iodine and cerium microspheres.

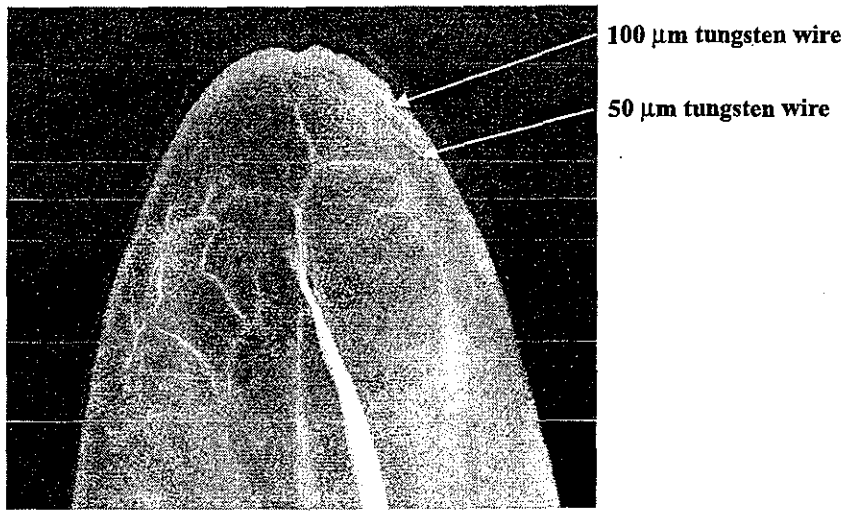

Figure 13: Angiograms of the external ear of a rabbit.

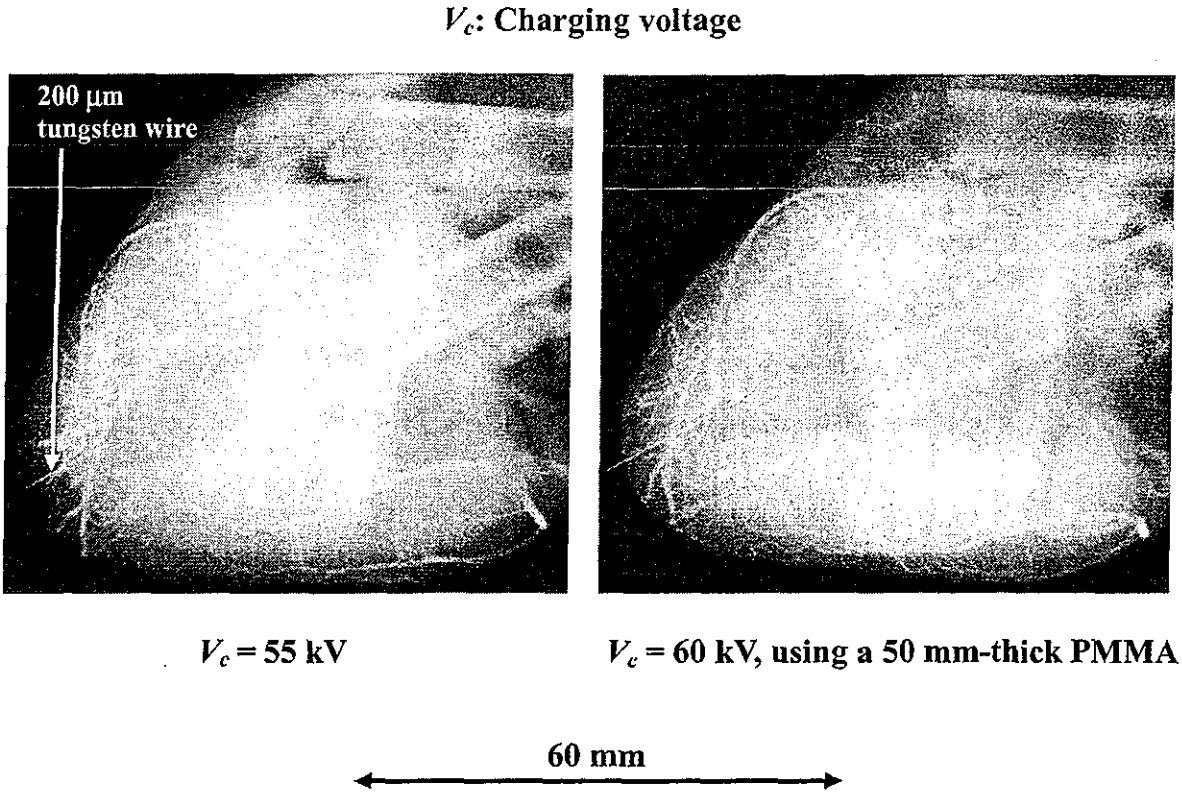

Figure 14: Angiograms of an extracted heart of a dog.

5. DISCUSSION

Cerium is a rare earth element and has a high reactivity. However, the average photon energy of K_α lines is 34.566 keV, and iodine spheres with a K-absorption edge of 33.155 keV absorb the lines easily (Fig. 15). Next, since the spheres easily transmit bremsstrahlung x-rays with energies of lower than the edge, it is important that the rays be absorbed as much as possible before angiography in order to increase the image contrast.

In an earlier experiment using a copper target,[23] bremsstrahlung x-rays were hardly observed at all, and we confirmed the irradiation of quite sharp and intense K-series characteristic x-rays such as lasers. In the present work, although we confirmed intense characteristic x-rays with a higher charging voltage, bremsstrahlung x-rays were detected, since the bremsstrahlung intensity is proportional to the atomic number of the target element. Therefore, the condenser charging voltage should be raised as high as possible to increase the characteristic x-ray intensity. In order to decrease emission of bremsstrahlung x-rays from the carbon target holder, the target length should also be set as long as possible.

In this research, we obtained sufficient x-ray intensity per pulse for CR radiography, and the generator produced high-dose-rate plasma x-rays of approximately 80 C/kg·s at 1.0 m with a charging voltage of 55 kV. In addition, because the x-ray intensity increases with increases in the electrostatic energy in the main discharge condenser, the flash x-rays from weakly ionized linear cerium plasma can be employed to perform high-speed angiography for cardiovascular disease.

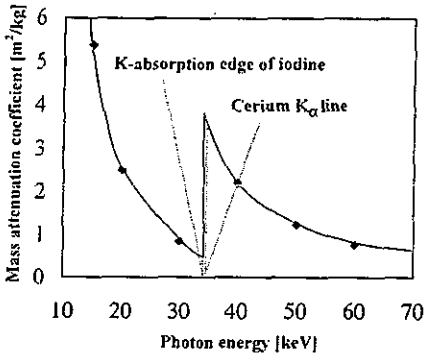

Figure 15: Relation between the mass attenuation coefficient of iodine and the average photon energy of cerium K_α lines.

ACKOWLEDGEMENTS

This work was supported by Grants-in-Aid for Scientific Research (12670902, 13470154, and 13877114) and Advanced Medical Scientific Research from MECSST, Grants from Keiryo Research Foundation, JST (Test of Fostering Potential), NEDO, and MHLW (HLSRG, RAMT-nano-001, RHGTEFB-genome-005, and RGCD13C-1).

REFERENCES

1. A. Mattsson, "Some characteristics of a 600 kV flash x-ray tube," *Physica Scripta*, **5**, pp. 99-102, 1972.

2. R. Germer, "X-ray flash techniques," *J. Phys. E: Sci. Instrum.*, **12**, pp. 336-350, 1979.

3. E. Sato, H. Isobe and F. Hoshino, "High intensity flash x-ray apparatus for biomedical radiography," *Rev. Sci. Instrum.*, **57**, pp. 1399-1408, 1986.

4. E. Sato, M. Sagae, K. Takahashi, T. Oizumi, H. Ojima, K. Takayama, Y. Tamakawa, T. Yanagisawa, A. Fujiwara and K. Mitoya, "High-speed soft x-ray generators in biomedicine," *SPIE*, **2513**, pp. 649-667, 1994.

5. E. Sato, M. Sagae, K. Takahashi, A. Shikoda, T. Oizumi, H. Ojima, K. Takayama, Y. Tamakawa, T. Yanagisawa, A. Fujiwara and K. Mitoya, "Dual energy flash x-ray generator," *SPIE*, **2513**, pp. 723-735, 1994.

6. E. Sato, M. Sagae, A. Shikoda, K. Takahashi, T. Oizumi, M. Yamamoto, A. Takabe, K. Sakamaki, Y. Hayasi, H. Ojima, K. Takayama and Y. Tamakawa, "High-speed soft x-ray techniques," *SPIE*, **2869**, pp. 937-955, 1996.

7. E. Sato, S. Kimura, S. Kawasaki, H. Isobe, K. Takahashi, Y. Tamakawa and T. Yanagisawa, "Repetitive flash x-ray generator utilizing a simple diode with a new type of energy-selective function," *Rev. Sci. Instrum.*, **61**, pp. 2343-2348, 1990.

8. S. Kimura, E. Sato, M. Sagae, A. Shikoda, T. Oizumi, K. Takahashi, Y. Tamakawa and T. Yanagisawa, "Disk-cathode flash x-ray tube driven by a repetitive two-stage Marx pulser," *Med. & Biol. Eng. & Comput.*, **31**, pp. S37-S43, 1993.

9. A. Shikoda, E. Sato, M. Sagae, T. Oizumi, Y. Tamakawa and T. Yanagisawa, "Repetitive flash x-ray generator having a high-durability diode driven by a two-cable-type line pulser," *Rev. Sci. Instrum.*, **65**, pp. 850-856, 1994.

10. E. Sato, K. Takahashi, M. Sagae, S. Kimura, T. Oizumi, Y. Hayasi, Y. Tamakawa and T. Yanagisawa, "Sub-kilohertz flash x-ray generator utilizing a glass-enclosed cold-cathode triode," *Med. & Biol. Eng. & Comput.*,

32, pp. 289-294, 1994.

11. K. Takahashi, E. Sato, M. Sagae, T. Oizumi, Y. Tamakawa and T. Yanagisawa, "Fundamental study on a long-duration flash x-ray generator with a surface-discharge triode," *Jpn. J. Appl. Phys.*, **33**, pp. 4146-4151, 1994.

12. E. Sato, A. Shikoda, S. Kimura, M. Sagae, H. Isobe, Y. Tamakawa and T. Yanagisawa, "Kilohertz-range flash x-ray generator utilizing a triode in conjunction with an extremely hot cathode," *Rev. Sci. Instrum.*, **62**, pp. 2115-2120, 1991.

13. E. Sato, M. Sagae, K. Takahashi, A. Shikoda, T. Oizumi, Y. Hayasi, Y. Tamakawa and T. Yanagisawa, "10 kHz microsecond pulsed x-ray generator utilizing a hot-cathode triode with variable durations for biomedical radiography," *Med. & Biol. Eng. & Comput.*, **32**, pp. 295-301, 1994.

14. E. Sato, T. Ichimaru, T. Usuki, K. Sato, H. Ojima, K. Takayama, H. Ido, K. Sakamaki and Y. Tamakawa, "Condenser-discharge stroboscopic x-ray generator SX-C98," *SPIE*, **3516**, pp. 618-625, 1998.

15. E. Sato. T. Ichimaru, H. Ojima, K. Takayama, H. Ido and Y. Tamakawa, "Characteristics of the kilohertz-range harder stroboscopic x-ray generator and applications," *SPIE*, **3771**, pp. 12-21, 1999.

16. E. Sato, T. Ichimaru, H. Obara, M. Zuguchi, H. Mori, E. Tanaka, T. Usuki, K. Sato, H. Ojima, K. Takayama, K. Sakamaki and Y. Tamakawa, "Condenser-discharge stroboscopic x-ray generator for medical radiography," *SPIE*, **4183**, pp. 383-393, 2000.

17. E. Sato, H. Ojima, K. Takayama, M. Matsumasa, H. Obara, M. Zuguchi, T. Usuki, K. Sato, K. Sakamaki and Y. Tamakawa, "Observation of cavitation bubble cloud using a stroboscopic x-ray generator," *SPIE*, **4183**, pp. 394-404, 2000.

18. E. Sato, Y. Hayasi and Y. Tamakawa, "Recent stroboscopic x-ray generators and their applications to high-speed radiography," *Ann. Rep. Iwate Med. Univ. Lib. Arts and Sci.*, **35**, pp. 1-11, 2000.

19. H. Mori, K. Hyodo, E. Tanaka, M.U. Mohammed, A. Yamakawa, Y. Shinozaki, H. Nakazawa, Y. Tanaka, T. Sekka, Y. Iwata, S. Honda, K. Umetani, H. Ueki, T. Yokoyama, K. Tanioka, M. Kubota, H. Hosaka, N. Ishizawa and M. Ando, "Small-vessel radiography in situ with monochromatic synchrotoron radiation," *Radiology*, **201**, pp. 173-177, 1996.

20. T.J. Davis, D. Gao, T.E. Gureyev, A.W. Stevenson and S.W. Wilkims, "Phase-contrast imagimg of weakly absorbing materials using hard x-rays," *Nature*, **373**, pp. 595-597, 1995.

21. A. Momose, T. Takeda, Y. Itai and K. Hirano, "Phase-contrast x-ray computed tomography for observing biological soft tissues," *Nature Medicine*, **2(4)**, pp. 473-475, 1996.

22. E. Sato, Y. Suzuki, Y. Hayashi, E. Tanaka, H. Mori, T. Kawai, K. Takayama, H. Ido and Y. Tamakawa, "High-intensity quasi-monochromatic x-ray irradiation from the linear plasma target," *SPIE*, **4505**, pp. 154-164, 2001.

23. E. Sato, Y. Hayashi, E. Tanaka, H. Mori, T. Kawai, H. Obara, T. Ichimaru, K. Takayama, H. Ido, T. Usuki, K. Sato and Y. Tamakawa, "Polycapillary radiography using a quasi-x-ray laser generator," *SPIE*, **4508**, pp. 176-187, 2001.

24. E. Sato, Y. Hayasi, E. Tanaka, H. Mori, T. Kawai, T. Usuki, K. Sato, H. Obara, T. Ichimaru, K. Takayama, H. Ido and Y. Tamakawa, "Quasi-monochromatic radiography using a high-intensity quasi-x-ray laser generator," *SPIE*, **4682**, pp. 538-548 2002.

25. E. Sato, Y. Hayasi, R. Germer, E. Tanaka, H. Mori, T. Kawai, H. Obara, T. Ichimaru, K. Takayama and H. Ido, "Intense characteristic x-ray irradiation from weakly ionized linear plasma and applications," *Jpn. J. Med. Imag. Inform. Sci.*, **20**, pp. 148-155. 2003.

26. E. Sato , K. Sato and Y. Tamakawa, "Film-less computed radiography system for high-speed Imaging," *Ann. Rep. Iwate Med. Univ. Sch. Lib. Arts and Sci.*, **35**, pp. 13-23, 2000.

Pediatric Cardiology

10.1007/s00246-004-0698-1

Incidence of Stenotic Lesions Predicted by Acute Phase Changes in Coronary Arterial Diameter During Kawasaki Disease

E. Tsuda[1] ✉, T. Kamiya[1], Y. Ono[1], K. Kimura[2], K. Kurosaki[2] and S. Echigo[1]

(1) Department of Pediatrics, National Cardiovascular Center, 5-7-1 Fujishirodai, Suita-shi, 565-8565 Osaka, Japan
(2) Department of Radiology, National Cardiovascular Center, 5-7-1 Fujishirodai, Suita-shi, 565-8565 Osaka, Japan

✉ **E. Tsuda**
Email: etsuda@hsp.ncvc.go.jp
Phone: 81-6-6833-5012
Fax: 81-6-6872-7486

Published online: 12 May 2004

Abstract To clarify the incidence of stenotic lesions according to the coronary arterial diameter in the acute phase. we investigated 190 patients with coronary arterial lesions who underwent an initial coronary angiogram (CAG) less than 100 days after the onset of Kawasaki disease. The largest diameters of the major branches were measured in the initial CAGs. The diameter of the large group was ≥8.0 mm, that of the medium group was ≥6.0 mm but <8.0 mm, and that of the small group was ≥ 4.0 mm but <6.0 mm. There were 121 patients in the large group, 85 in the medium group, 77 in the small group. We investigated the stenotic lesions in the follow-up CAGs and evaluated the incidence of stenotic lesions in each group by the Kaplan–Meier method. The mean interval from the initial CAGs to the latest CAG was 97 months. The incidence of stenosis at 5, 10, and 15 years in the large group was 44, 62, and 74%, respectively. In the medium group the corresponding values were 6, 20, 58%, respectively. None of the patients in the small group developed stenotic lesions. Dilatation of more than 6.0 mm produces a high probability of irreversible change in the coronary arterial wall, leading to subsequent stenotic lesions.

Keywords Kawasaki disease - Coronary artery disease - Stenotic lesions

Although 35 years have passed since the first description of Kawasaki disease (KD), its long-term prognosis remains unclear [8, 9]. Although some reports of the midterm fate of coronary arterial lesions after KD exist, the incidence of stenotic lesions previously reported is that of the whole coronary arterial distribution [1, 5, 6, 7, 13, 16, 18], and it is generally accepted that aneurysms exceeding 8.0 mm evolve into stenotic lesions [11, 21]. However, it is questionable how large an aneurysm results in a stenotic lesion. Stenotic lesions are the most important coronary arterial lesions due to KD because they induce myocardial ischemia and myocardial infarction, and myocardial infarction highly influences the prognosis [17]. We speculated that the fate of coronary arterial lesions, including the development of coronary stenosis after KD, relates to the degree of coronary arterial dilatation during the acute phase. Therefore, we tried to clarify the incidence of subsequent stenosis and the incidence of

regression of coronary dilatation according to the coronary arterial diameter during the acute phase in both branch lesions and bifurcation lesions. Such data should clearly indicate the stratification of coronary arterial lesions and help the long-term management of patients with coronary arterial lesions due to KD.

Patients and Methods

Patient Population

We investigated 190 patients with coronary arterial lesions who underwent an initial selective coronary angiogram less than 100 days after the acute onset of KD. All were seen since 1978. All patients gave informed consent for selective coronary angiography, and all patients had coronary artery dilatation ≥3.0 mm in one or more branches and had undergone coronary angiography at least twice. There were 142 males and 48 females. The age at the onset ranged from 3 months to 13 years. The mean age at the onset of KD was 33 ± 30 months. The distribution of patients by age of onset was as follows: 0 year, 59; 1 year, 37; 2 years, 32; 3 years, 15; 4 years, 17; 5 years, 11; 6 years, ≤19. A total of 160 patients (84%) were younger than 5 years old at the age of onset.

With regard to treatment during the acute phase of KD, 86% of patients received aspirin, and intravenous immunoglobulin was administered in 40% at a dose of 1–2 g/kg.

During the follow-up period, 90% of patients received antiplatelet agents, and 26% received warfarin. Aspirin dosage used was 1.5–3.0 mg/kg. When aneurysms of both coronary arteries regressed, the drugs were discontinued (46% of patients).

Methods

The mean interval from the onset of KD to the initial coronary angiogram was 58 ± 20 days. All patients underwent a second coronary angiogram after an interval of 1 year. Subsequent follow-up coronary angiograms were performed at 3- to 5-year intervals depending on the previous findings. If the coronary aneurysm regressed, subsequent coronary angiograms were not performed. Such patients were followed in the outpatient clinic by noninvasive imaging, including cardiac echocardiography and electron beam computed tomography. If coronary arterial lesions were suspected on noninvasive imaging, coronary angiography was considered at that time. However, for acute phase giant coronary aneurysms with apparent regression, coronary angiograms were still performed in the late period up to more than 10 years later. The mean number of coronary angiogram studies was 4 ± 2, with a mean interval from the onset of KD to the latest coronary angiogram of 96.9 ± 72.3 months. The maximum interval was 250 months.

We categorized branch stenotic lesions and their regression in the follow-up coronary angiograms in groups based on the coronary arterial diameter in the initial coronary angiogram. We assessed localized aneurysms at the bifurcation of the left coronary artery separately from the major branches because of their characteristics. In this study, a bifurcation lesion indicates an aneurysm at the bifurcation of the left coronary artery that does not extend into the left anterior descending artery or the left circumflex.

We considered the first appearance of stenosis an event and evaluated its incidence in each group by the Kaplan–Meier method, which we also used to evaluate the incidence of regression of coronary dilatation in each group. The data were compared by the Cox–Mantel examination, and a significant difference was accepted as being less than 5%.

For this study, a stenotic lesion was defined as localized stenosis ≥25%, segmental stenosis, or complete occlusion. If acute myocardial infarction occurred and the occluded branch was diagnosed on electrocardiogram or on angiogram after the episode, it was considered as the event. For bifurcation lesions, we considered the appearance of a stenotic lesion in the left anterior descending artery, the left circumflex, or the left main trunk as an event. Regression was defined as regression of all coronary aneurysms in the respective branches or at the bifurcation.

We measured the largest diameters of the right coronary artery and the left anterior descending and the left circumflex arteries in the initial coronary angiograms, as previously described [23]. These made up the branches groups. The diameters of the right coronary artery were measured in the left anterior oblique 60° view, whereas the diameters of the left anterior descending artery and the circumflex were measured in the right anterior oblique 30° or right anterior oblique 30° with caudal angulation of 30°. The diameters of the circumflex were measured in the left anterior oblique 60° view with 30° cranial regulation. Bifurcation lesions of the left coronary artery were measured in a right anterior oblique 30° view with caudal 30° angulation. The measured diameters are shown in Fig. 1. The measured optimal angiogram was selected by both observers. The maximum diameters were measured using a software program (Siemence Ancor Version 2.3.1). Measurements by each observer and between observers were reproducible with high correlation coefficients, as previously published [23].

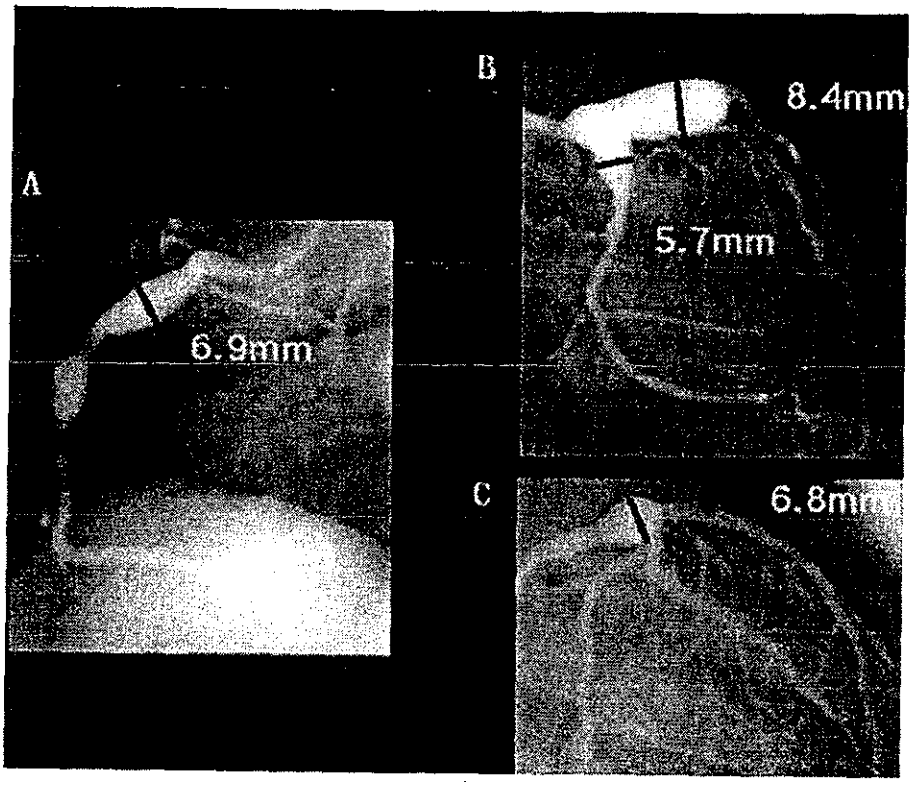

Figure 1 Measurement of coronary arterial diameter in the initial angiogram. (**A**) Right coronary artery. (**B**) Left anterior descending artery and left circumflex artery. (**C**) Bifurcation lesion of the left coronary artery.

Branch and bifurcation lesions were classified into three groups according to their largest diameter. The diameter of the large group (L) was ≥8.0 mm. That of the medium group (M) was ≥6.0 mm but <8.0 mm, and that of the small group (S) was ≥ 4.0 mm but <6.0 mm. For branch lesions, the numbers in the respective groups were as follows: L, 121; M, 85; and S, 77. For left bifurcation lesions, the numbers in the respective groups were as follows: L, 18; M, 25; and S, 34. The number of patients in the branch group in which the diameter was ≥3.0 mm but <4.0 mm was 59, and for bifurcation lesions there were 9 patients. The mean intervals from the onset of KD to the latest coronary angiogram for the respective groups are shown in Table 1. The unpaired *t* test was used to compare the medium group with the large group for branch lesions. One-factor analysis of variance was used to compare groups for the

bifurcation lesions. A significant difference was accepted as being less than 5%.

Table 1 Groups based on coronary artery diameter in the acute phase

Diameter (mm)	Group	*n*	RCA	LAD	LCX	Interval from the onset to the latest coronary angiogram (months)	
						Mean	SD
Branch group							
≤3.0 but <4.0		59	18	19	22	72	65
≤4.0 but <6.0	Small	77	31	29	17	83	68
≤6.0 but <8.0	Medium	85	38	35	12	112	71
≤8.0	Large	121	65	45	11	117	73
Bifurcation lesion							
≤3.0 but <4.0		9				120	88
≤4.0 but <6.0	Small	34				91	74
≤6.0 but <8.0	Medium	25				102	71
≤8.0	Large	15				110	74

RCA, right coronary artery; LAD, left anterior descending artery; LCX, left circumflex artery.

Results

For the branches, the incidence of stenotic lesions in the respective groups is shown (Fig. 2). The incidence of stenotic lesions at 5, 10, and 15 years in the large group was 44, 62, and 74%, respectively. The incidence of stenotic lesions at 5, 10, and 15 years in the medium group was 6, 20, and 58%, respectively. The incidence of stenotic lesions in the large group is significantly greater than that in the medium group ($p < 0.01$). No aneurysms <6.0 mm in diameter in both the branch group and the bifurcation group developed stenotic lesions. The threshold diameter for acute phase coronary aneurysms leading to subsequent stenosis was 6.0 mm.

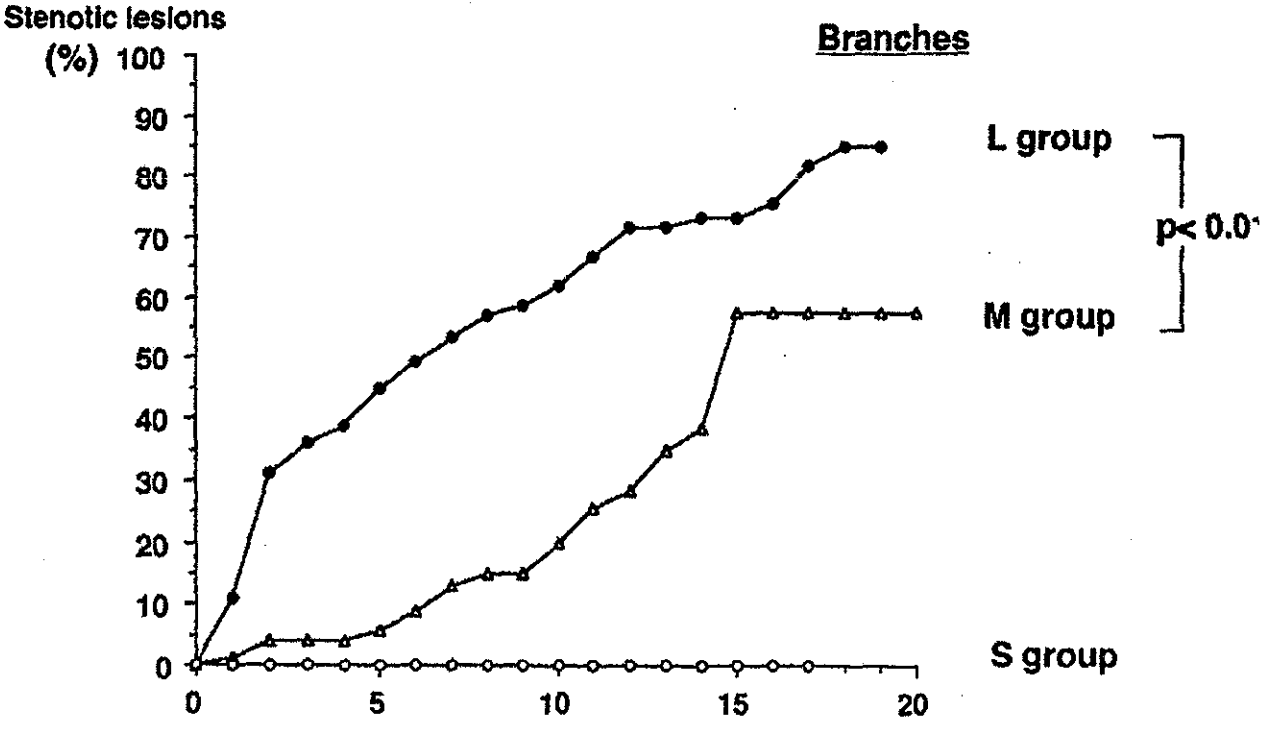

years

Figure 2 Incidence of coronary stenotic lesions bated on coronary diameter in the acute phase (branches).

The incidence of complete occlusion in the branches in the respective groups is shown Fig. 3, and at 5, 10, and 15 years in the large group it was 30, 43, and 45%, respectively. In the medium group; at 5, 10, and 15 years it was 1, 8, and 15%, respectively. The incidence of occlusion in the large group is significantly greater than that in the medium group ($p < 0.01$).

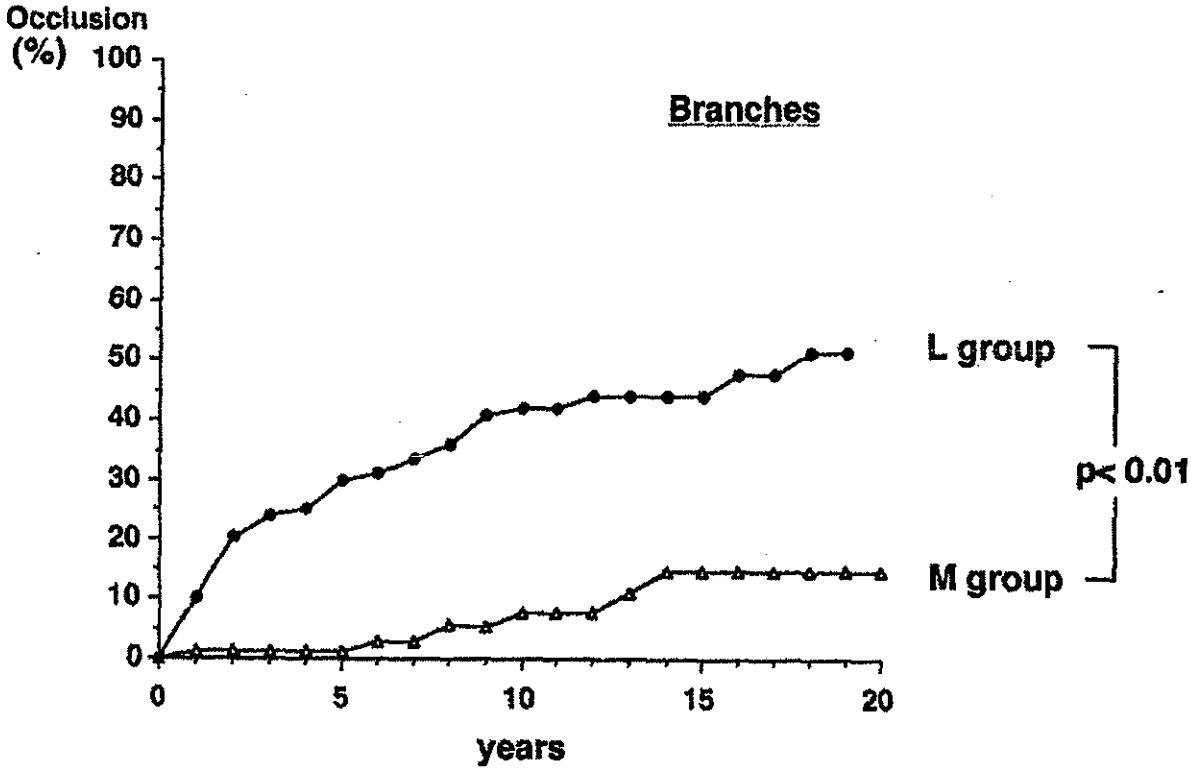

Figure 3 Incidence of coronary arterial occlusion based on coronary diameter in the acute phase (branches).

For bifurcation lesions of the left coronary artery, the incidence of stenotic lesions in the respective groups is shown in Fig. 4. After 15 years, the incidence of stenotic lesions in the medium and large groups was 13 and 23%, respectively. This was low compared with that of the branch groups.

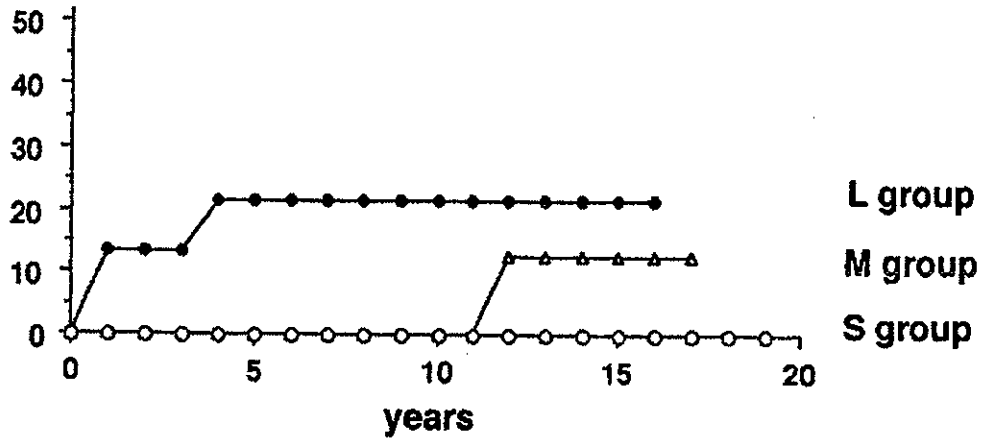

Figure 4 Incidence of coronary stenotic lesions based on coronary diameter in the acute phase (bifurcation lesions).

The incidence of regression of coronary dilatation was also evaluated for both branch and bifurcation lesions. All aneurysms <4.0 mm in diameter for both branch and bifurcation lesions regressed. Regression of coronary dilatation was evaluated in the branch group (Fig. 5). Its incidence at 5, 10, and 15 years in the small group was 74, 80, and 86%, respectively; in the medium group it was 26, 32, and 35%, respectively; and in the large group it was 6, 8, and 8%, respectively. The incidence of regression of coronary dilatation in the medium group was significantly greater than that in the large group ($p < 0.01$).

Figure 5 Incidence of regression of coronary arterial dilatation based on coronary diameter in the acute phase (branches).

For bifurcation lesions (Fig. 6), after 15-year follow-up, the incidence of regression in the small, medium, and large groups was 80, 67, and 23%, respectively. The incidence of regression of coronary dilatation in the medium group was significantly greater than that in the large group ($p < 0.05$).

Figure 6 Incidence of regression of coronary arterial dilatation based on coronary diameter in the acute phase (bifurcation lesions).

We mapped the fate of coronary arterial dilatation based on the coronary arterial diameter in the acute phase from the previously mentioned data (Fig. 7). Of the patient population we studied, 186 patients are alive and 4 patients have died. Myocardial infarction occurred in 18 branches.

Figure 7 Fate maps of coronary arteries based on coronary diameter in the acute phase.

Discussion

In a national survey of KD in Japan in 1999 and 2000, 15,104 patients were reported. The survey revealed that coronary artery aneurysms developed in 17.16% of patients within 1 month of the onset of KD. Giant aneurysms, aneurysms, and dilatations occurred in 0.46, 2.60, and 14.10% of patients, respectively. However, 1 month after the onset, aneurysms were present in only 5.67% (giant, 0.40%; aneurysms, 1.87%; and dilatations 3.40%) [24]. We estimate that late cardiac sequelae currently affect approximately 1% of KD patients.

The degree of coronary arterial dilatation most likely determines the subsequent fate of the vessel. Stenotic lesions include localized stenosis and complete occlusion. Localized stenosis is mainly caused by thickening of the vessel walls [3, 23], and we have shown a significant correlation between the diameters of coronary arteries in the acute phase of KD measured at coronary angiography and subsequent intima-medial thickness observed more than 10 years later [13]. The degree of coronary arterial dilatation depends on the degree of destruction of the coronary arterial wall, and the extent of subsequent intimal thickening varies depending on the degree of injury during the acute phase, not only in a given patient but also in a given branch. Intimal thickening should be considered part of the reparative stage of the coronary arterial wall after the acute inflammation. The degree of destruction of the coronary arterial wall will determine the fate of the coronary arterial lesion. In a given patient, the coronary artery abnormalities change with time, and between patients the rate of change is variable.

The fate of coronary arterial dilatation can be divided into three major possibilities; persistent dilatation, regression, or progressive stenosis. The partition among the three major possibilities depends on the initial coronary artery diameter in the acute phase of KD. Acquired ischemic heart disease after KD is mainly caused by stenotic lesions [12]. However, persistent dilatation and regression of large coronary aneurysms can cause acute coronary infarction. We determined the fate of coronary arterial lesions, with our focus on the initial coronary artery diameter.

In the branch group, we found that dilatation of more than 6.0 mm results in a high probability of irreversible change in the coronary arterial wall, leading to subsequent stenosis or occlusion. In the large group, the incidence of stenosis was high at 5- and 15-year follow-up. In the medium group, although the incidence of stenosis was low at 5-year follow-up, it was much higher after 15 years. Although in most cases stenosis gradually develops through intimal thickening of the vascular wall over many years [3, 12, 15, 19, 22, 23], occlusion often occurred due to thrombotic events within approximately 2 years after the onset of KD. Impaired endothelial function that predisposes to thrombosis is possibly severe when coronary arterial dilatation exceeds 8.0 mm.

With respect to regression, after 15 years, its incidence in the small group, the medium group, and the large group was 86, 35, and 8%, respectively. The smaller the coronary artery diameter in the acute phase, the greater the probability of regression. As with stenotic lesions, the regression of coronary artery lesions depends on the original degree of coronary arterial dilatation.